ECMWF Training Course Notes
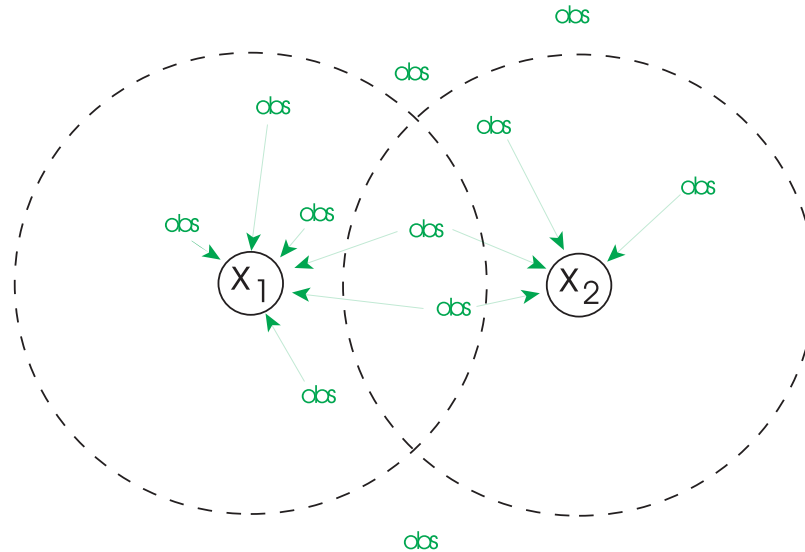

Figure 9. One OI data selection strategy is to assume that each analysis point is only sensiti ve to observations located in a small vicinity. Therefore, the observations used to perform the analysis at two neighbouring points x_1 or x_2 may be different, so that the analysis ḟeld will generally not be continuous in space. The cost of the analysis increases with the size of the selection domains.
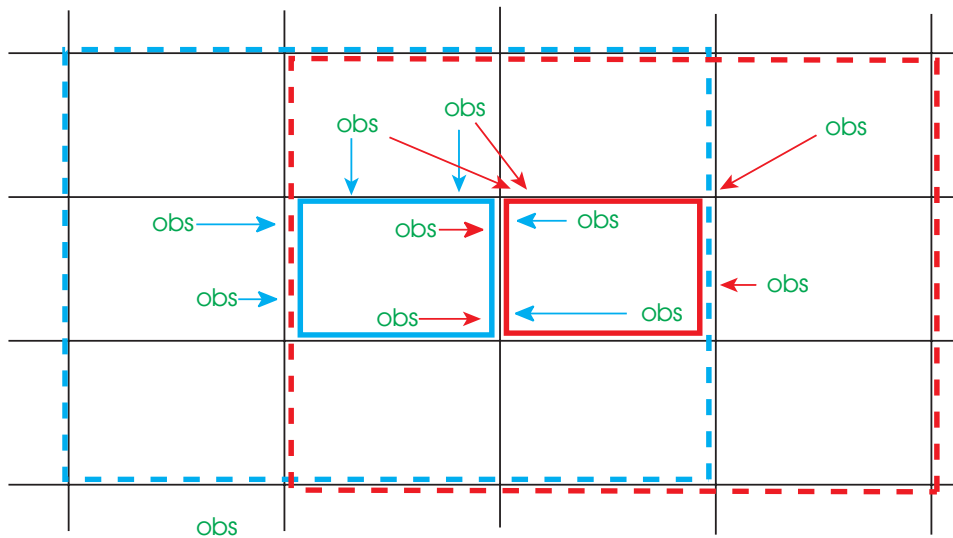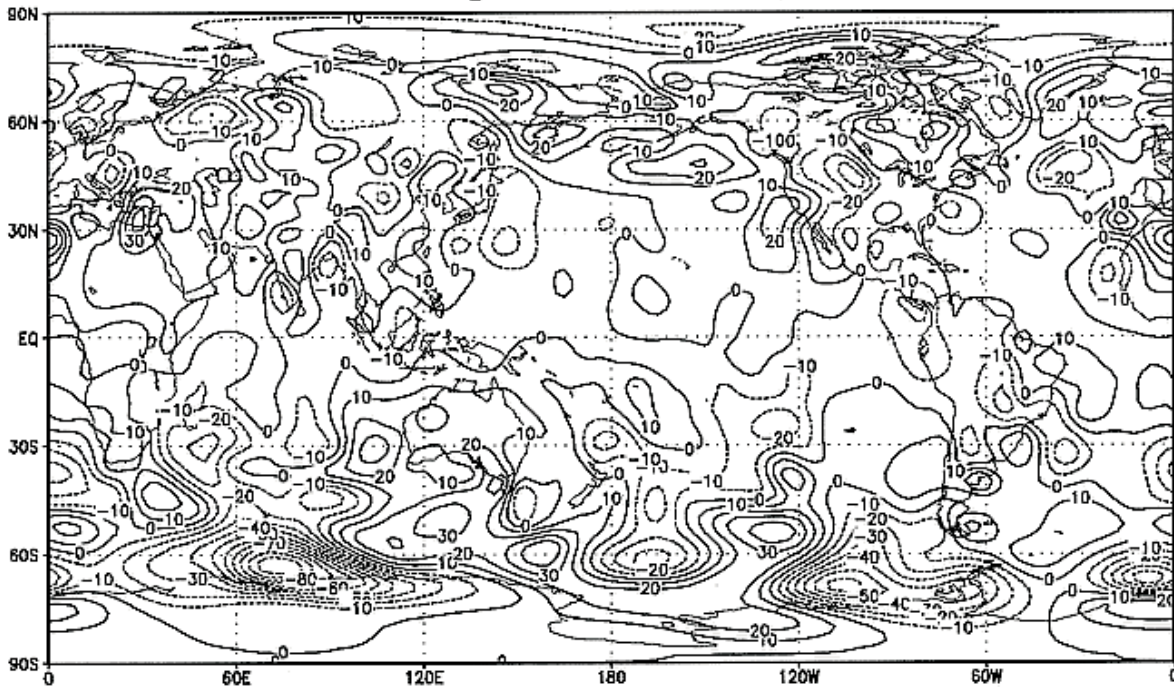

Figure 10. A slightly more sophisticated and more e xpensive OI data selection is to use, for all the points in an analysis box (black rectangle), all observations located in a bigger selection box (dashed rectangle), so that most of the observations selected in two neighbouring analysis box es are identical.

The advantage of OI is its simplicity of implementation and its relatively small cost if the right assumptions can be made on the observation selection.
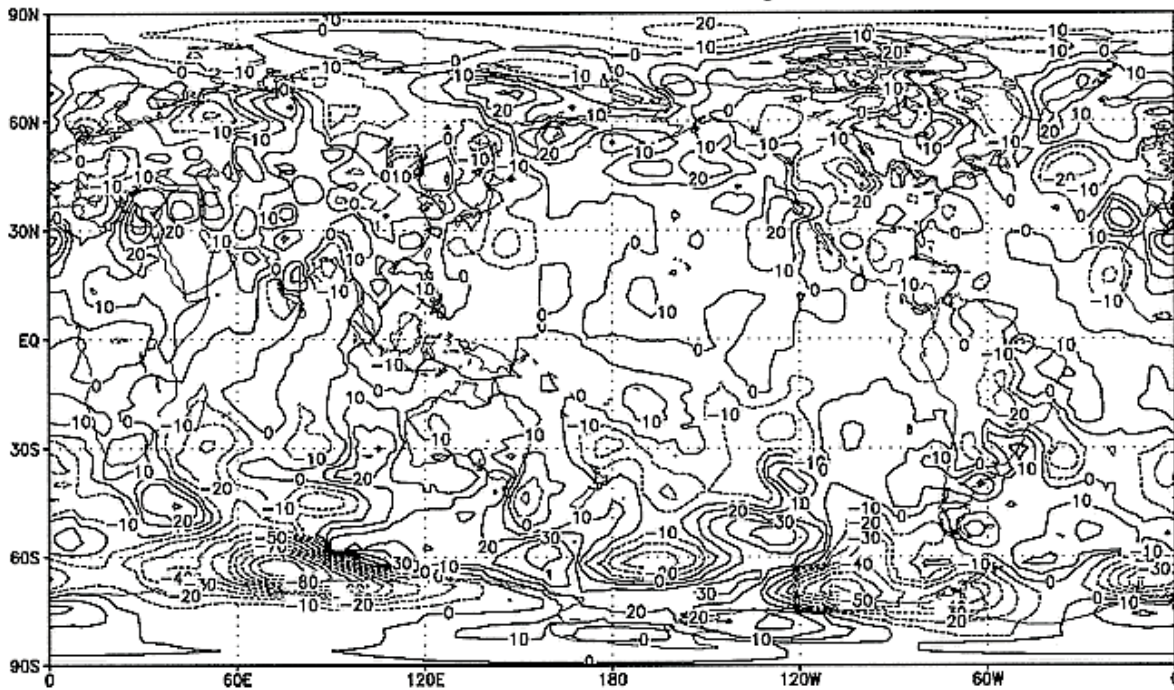
height 500 mb

Fig. 2. Height analysis increments at 500 hPa for 1200 UTC 28 August 1985 (case 1) produced with PSAS (top panel) and GEOS-1 OI (bottom panel). Contour interval: 10 m.

Cohn et al. (1998)
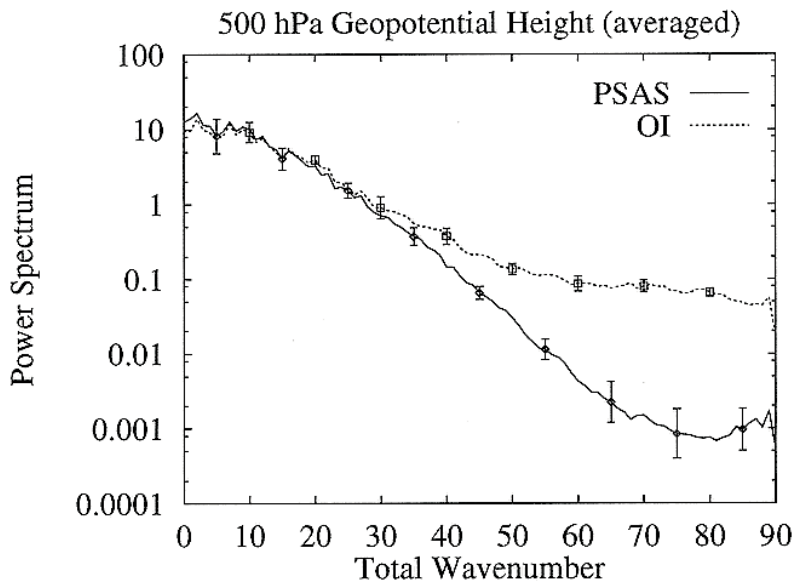
500 hPa Geopotential Height (averaged)

Fig. 3. Power spectra as a function of spherical harmonic total wavenumber for PSAS (solid line) and OI (dashed line) analysis increments of geopotential height at 500 hPa (five-case average, see Table 1). Bars indicate the range of the spectra among the five cases. Units: m^2.
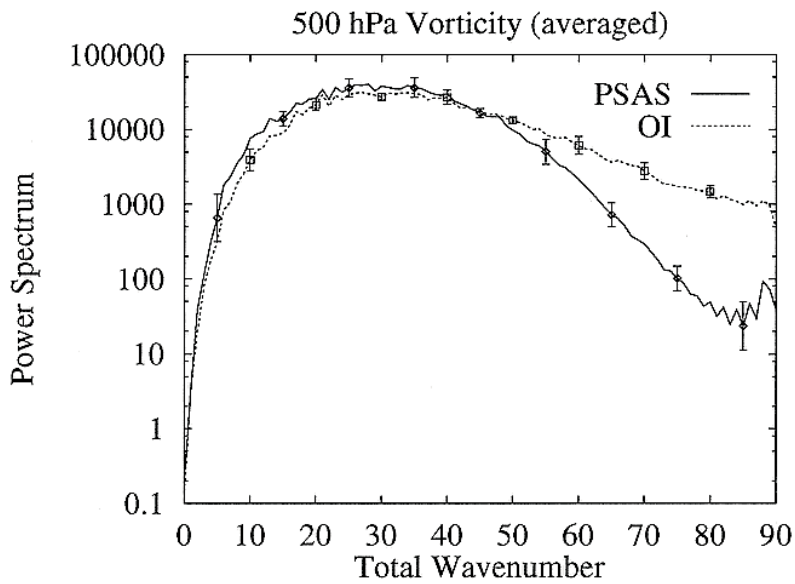
500 hPa Vorticity (averaged)

Fig. 4. As in Fig. 3 but for 500-hPa relative vorticity. Units: $10^{-15}s^{-2}$.

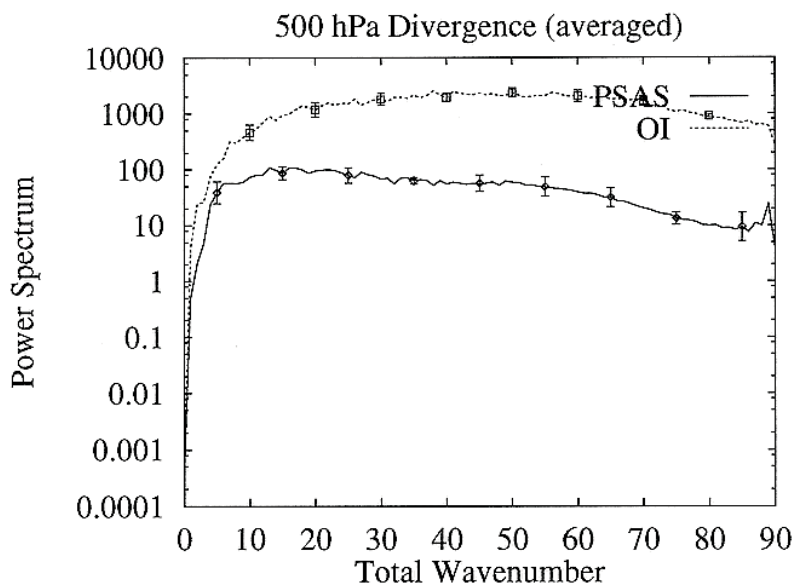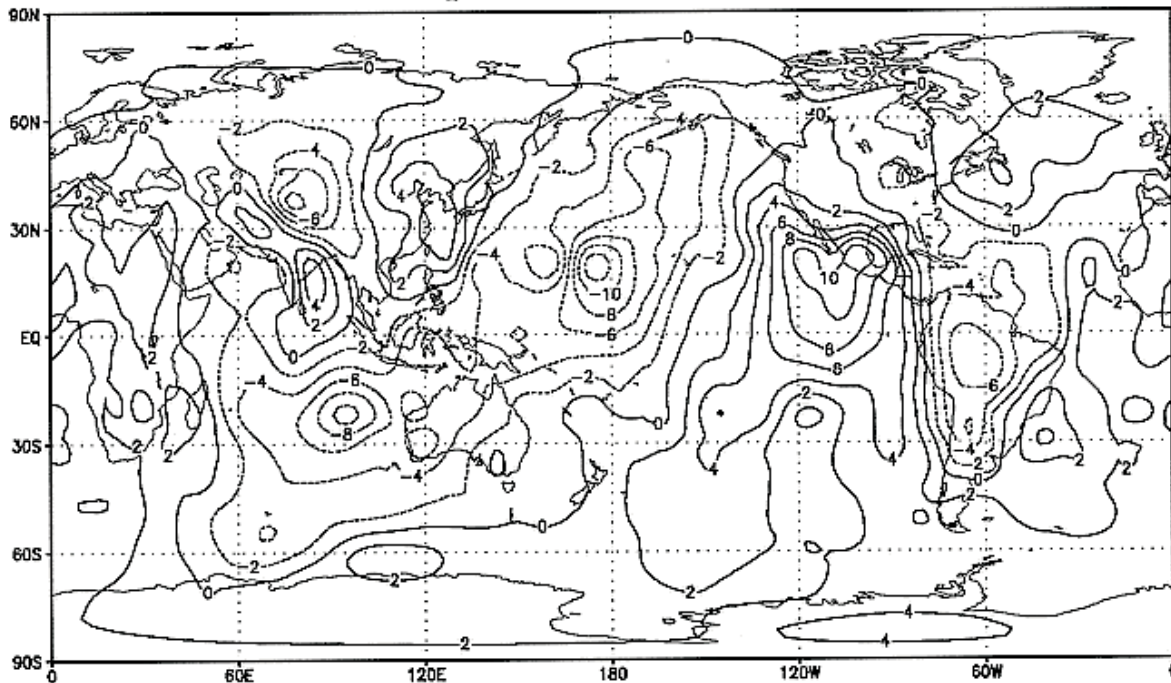## 500 hPa Divergence (averaged)

Fig. 5. As in Fig. 3 but for 500-hPa divergence. Units: $10^{-15}s^{-2}$.

Cohn et al. (1998)

Streamfunction 200 mb

200 hPa CHI (psas0101: 28 Aug 1985, 12 Z)

PSAS

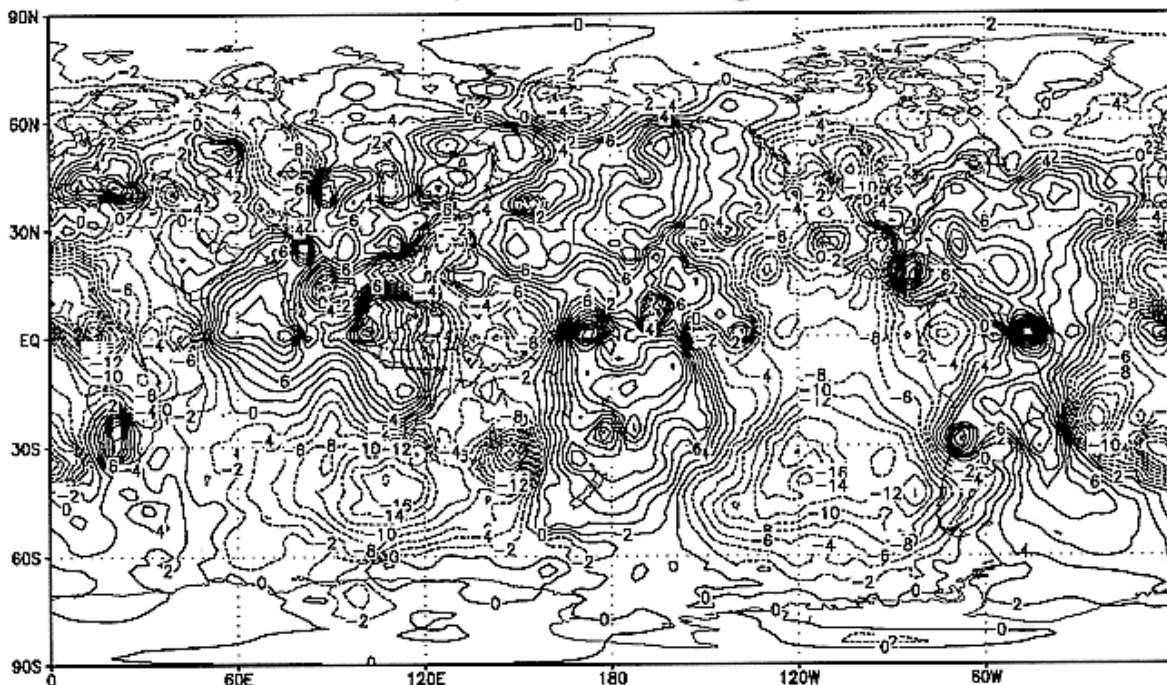## 200 hPa CHI (e0054A: 28 Aug 1985, 12 Z)

OI

Fig. 6. Velocity potential analysis increments at 200 hPa for 1200 UTC 28 August 1985 (case 1) produced with PSAS (top panel) and GEOS-1 OI (bottom panel). Normalization is by the factor ($2\Omega \sin 45\ g^{-1}$), where Ω is the earth's rotation rate and g is the gravity constant. Contour interval: 2 m.

Cohn et al. (1998)
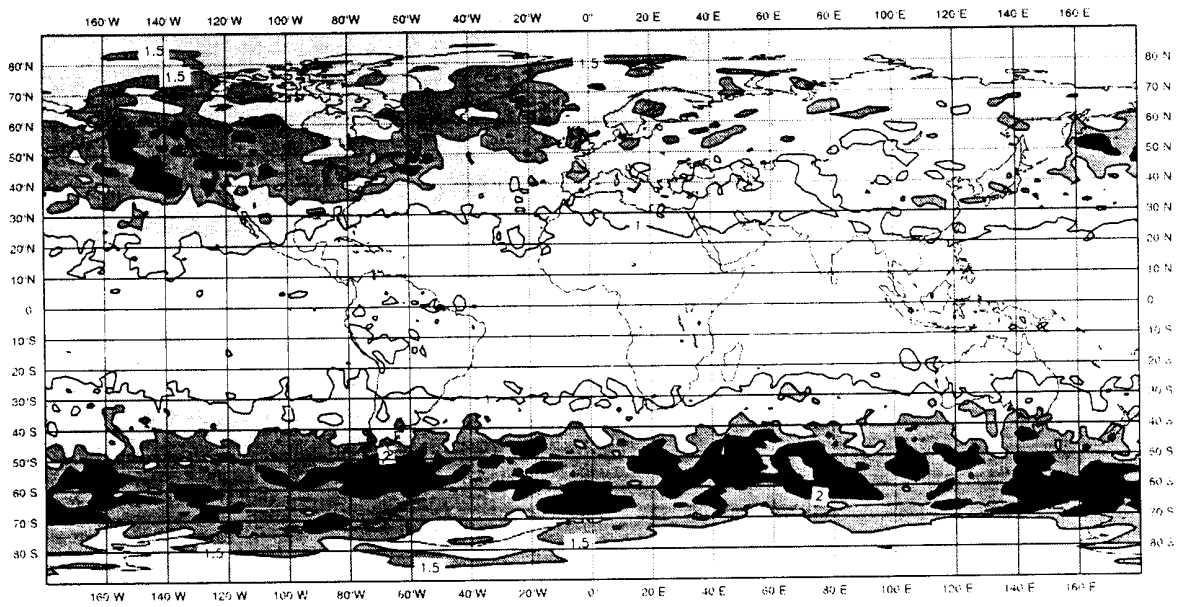
Figure 2. Geographical distribution of standard deviations obtained from the accumulation of three months of statistics (December, January and February) for the temperature at level 18 (approximately 500 hPa). Contours are at 0.5 K intervals. (There are some small areas in the tropics where values are a little below 0.5 K. The 0.5 K contours around them are not labelled.)
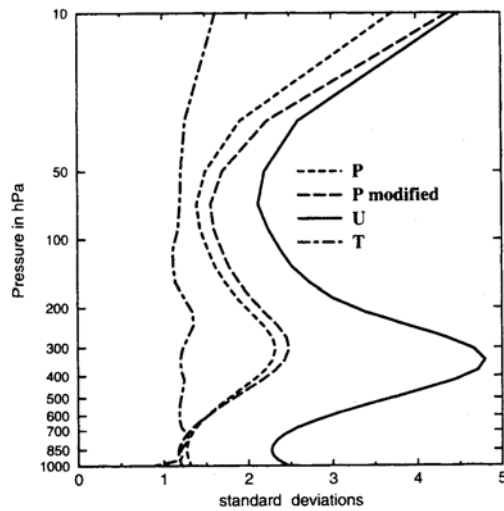
Rabier et al. (1998)

Figure 1. Horizontally averaged standard deviations as a function of pressure (hPa) for the mass variable P (dashed line) (100 $m^2 s^{-2}$), mass variable modified as explained in section 4 of the text (long-dashed line) (100 $m^2 s^{-2}$), wind components (solid line) ($m s^{-1}$) and temperature (dash-dotted line) (K).
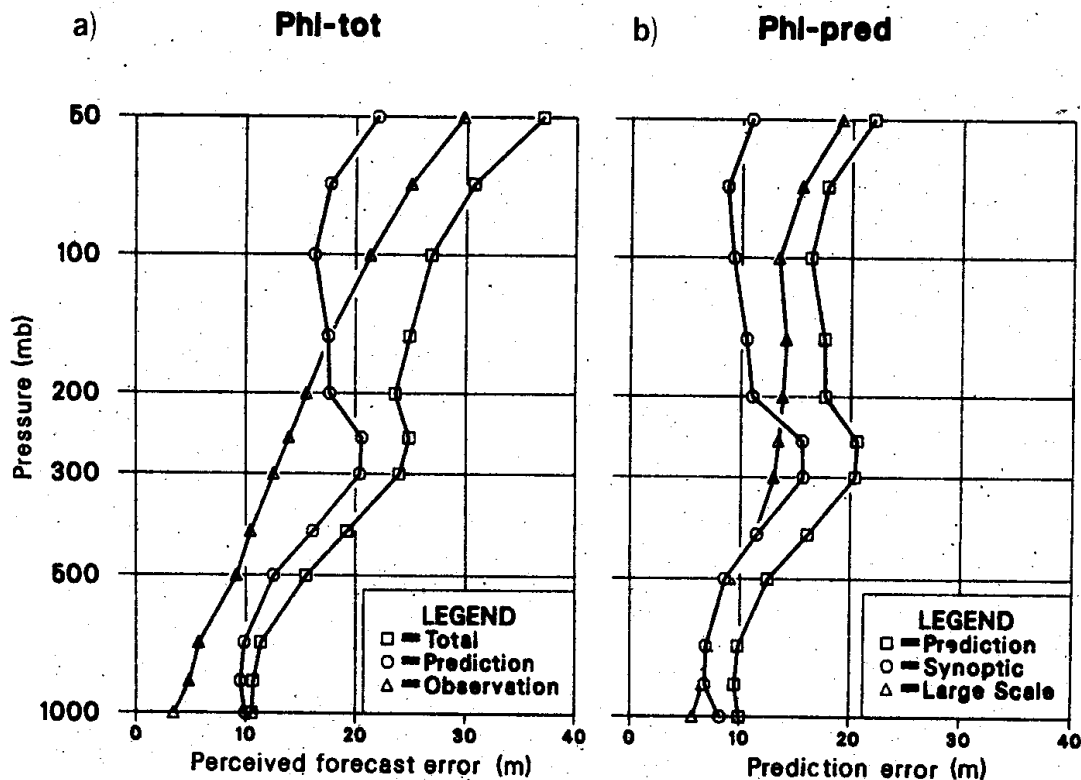
Rabier et al. (1998)

Fig. 2. (a) Vertical profiles of the total, or perceived, forecast error of height, together with the contributions to this error from prediction error, and the observation error. The unit is metres. (b) Vertical profiles of the prediction error (copied from 2a) and of the contributions of the synoptic-scale and large-scale components to the prediction error. The sum of the squares of the components gives the square of the prediction error.
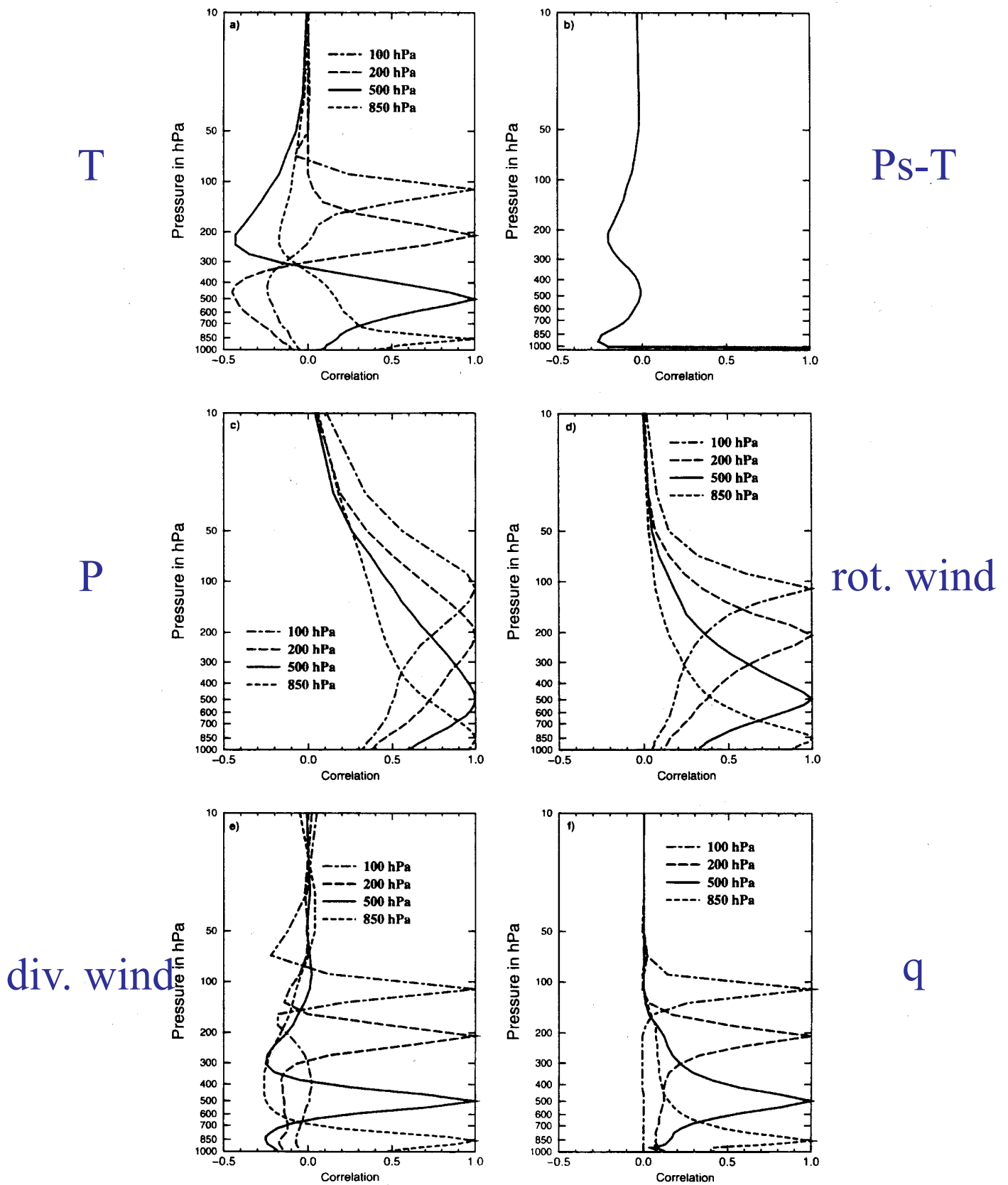
Lonnberg and Hollingsworth (1986)

T

Ps-T

P

rot. wind

div. wind

q

Figure 8.   Global vertical correlations as a function of pressure (hPa) for four selected model-levels: (a) temperature T; (b) cross-correlation between surface pressure (represented by the lowest point on the curve) and temperature; (c) the mass variable P; (d) rotational part of the wind; (e) divergent part of the wind; (f) specific humidity Q. Level 6 (approximately 100 hPa) is denoted by a dash-dotted line, level 10 (approximately 200 hPa) by a long-dashed line, level 18 (approximately 500 hPa) a solid line and level 26 (approximately 850 hPa) a dashed line.
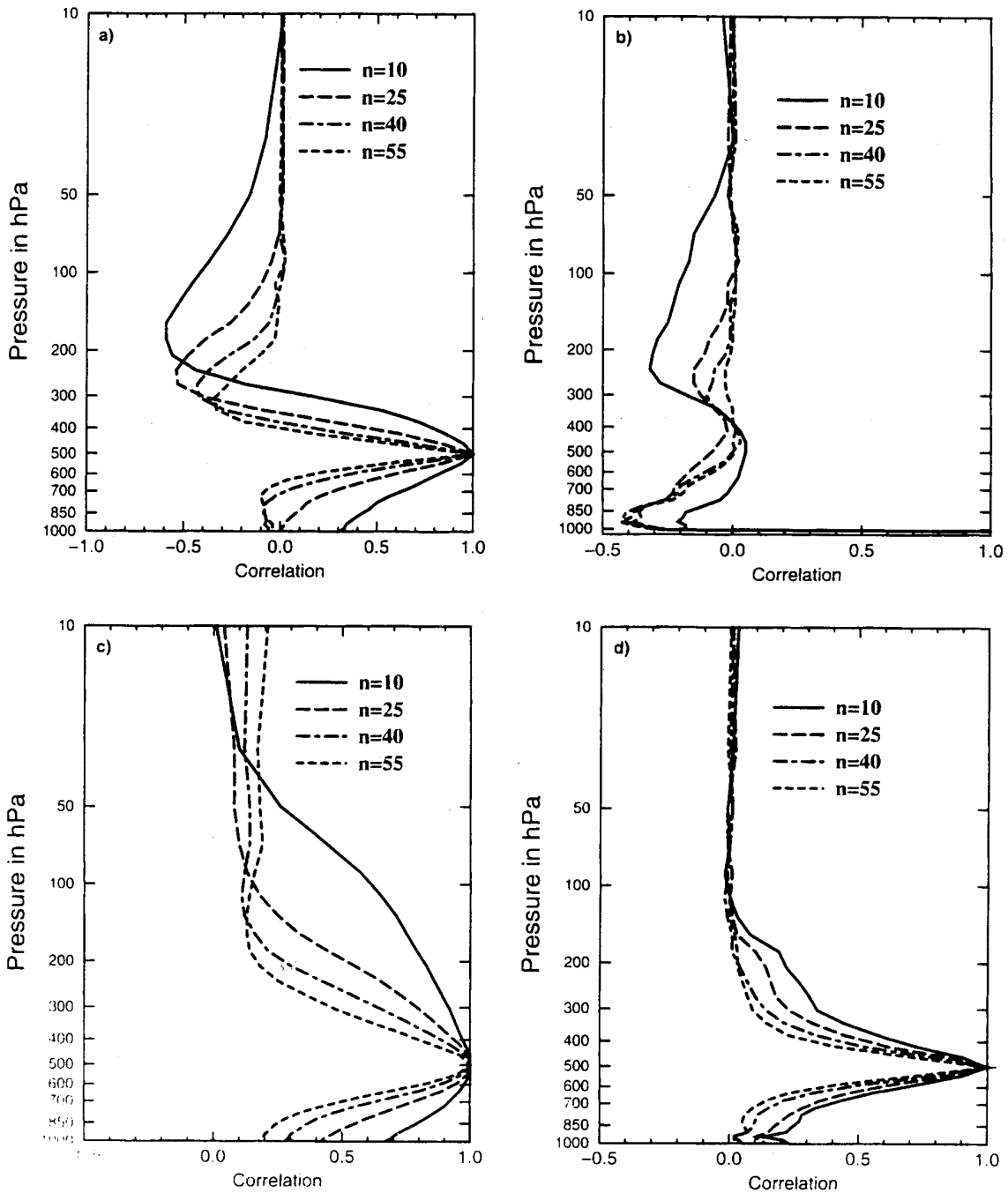
Rabier et al. (1998)

Figure 9.   Vertical correlations for level 18 (approximately 500 hPa) as a function of pressure (hPa) for selected horizontal wave-numbers: (a) temperature T; (b) cross-correlation between surface pressure (represented by the lowest point on the curve) and temperature; (c) the mass variable P; (d) specific humidity Q. Wave numbers 10, 25, 40 and 55 are shown by solid, long-dashed, dash-dotted and dashed lines respectively.
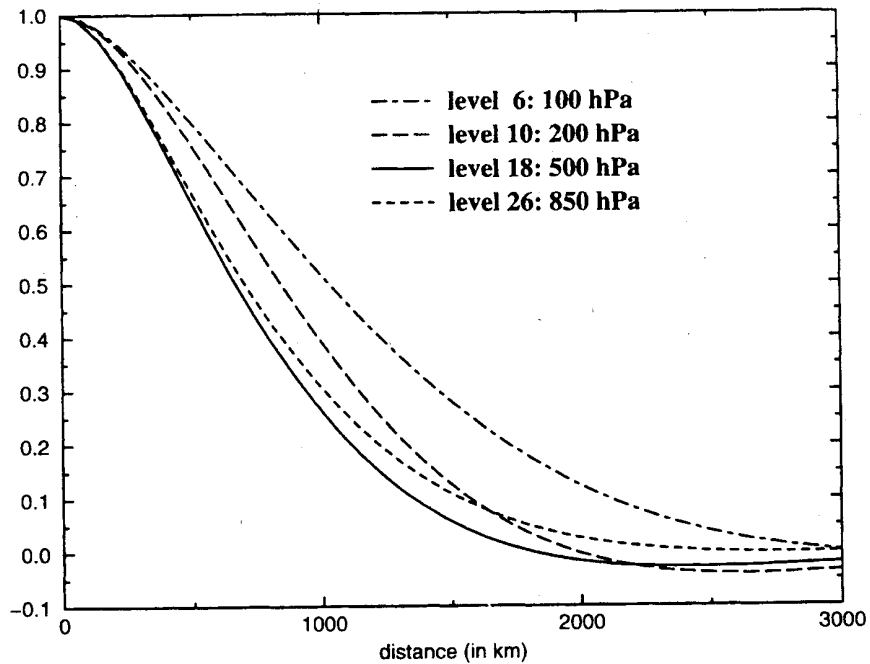
Rabier et al. (1998)

Figure 4. Horizontal autocorrelations as a function of horizontal distance for the mass variable P and selected model-levels. Level 6 (approximately 100 hPa) is denoted by a dash-dotted line, level 10 (approximately 200 hPa) by a long-dashed line, level 18 (approximately 500 hPa) a solid line and level 26 (approximately 850 hPa) a dashed line.
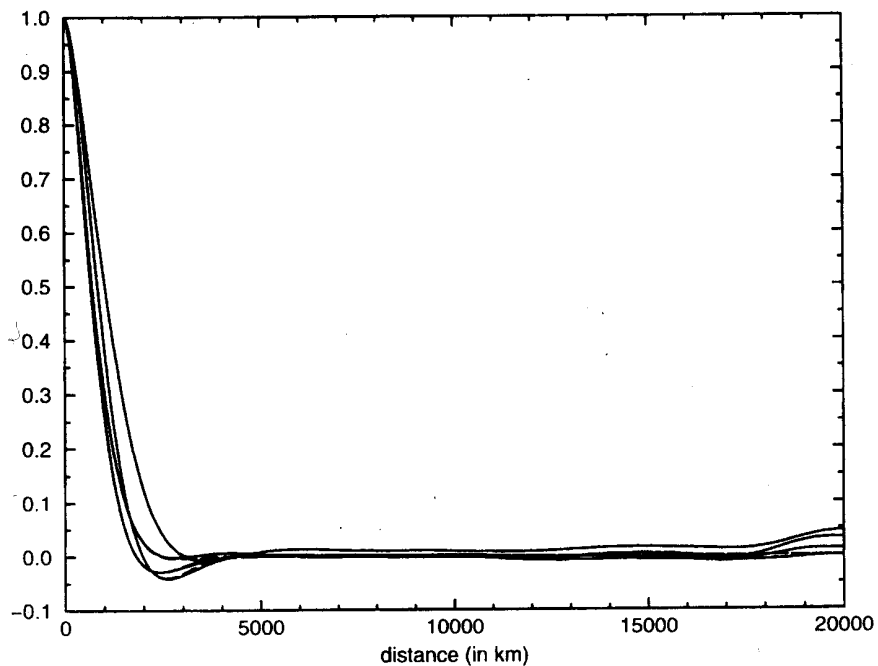
Rabier et al. (1998)

Figure 5. Horizontal autocorrelations as a function of horizontal distance up to large distances for the mass variable P and selected model-levels: original curves (solid lines); compactly supported correlations obtained by resetting the correlations to zero after 4000 km (dashed lines). The four levels are almost indistinguishable in this plot. Compare Fig. 4.
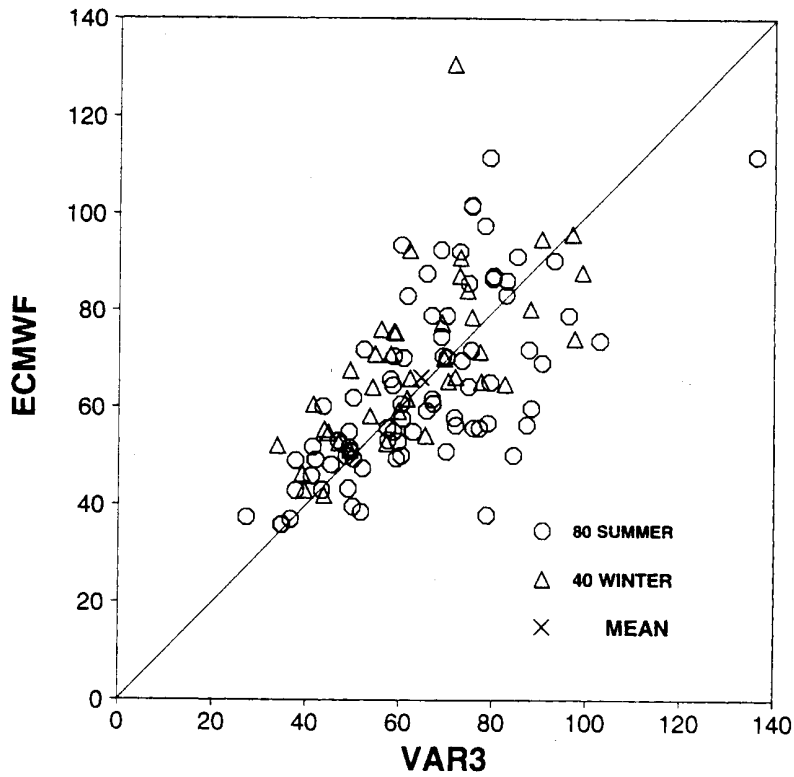
Rabier et al. (1998)

Figure 4. Scatter diagram of r.m.s. error (m) of forecasts of geopotential at 500 hPa for 120 days at 12 UTC in three separate periods (5 April 1995–14 May 1995, 24 August 1995–28 October 1995, 16 January 1996–29 January 1996), for 3D-Var (x-axis) and OI (y-axis). The 40 winter cases are denoted by triangles and the 80 summer cases by circles. The cross indicates the mean.

Andersson et al. (1998)

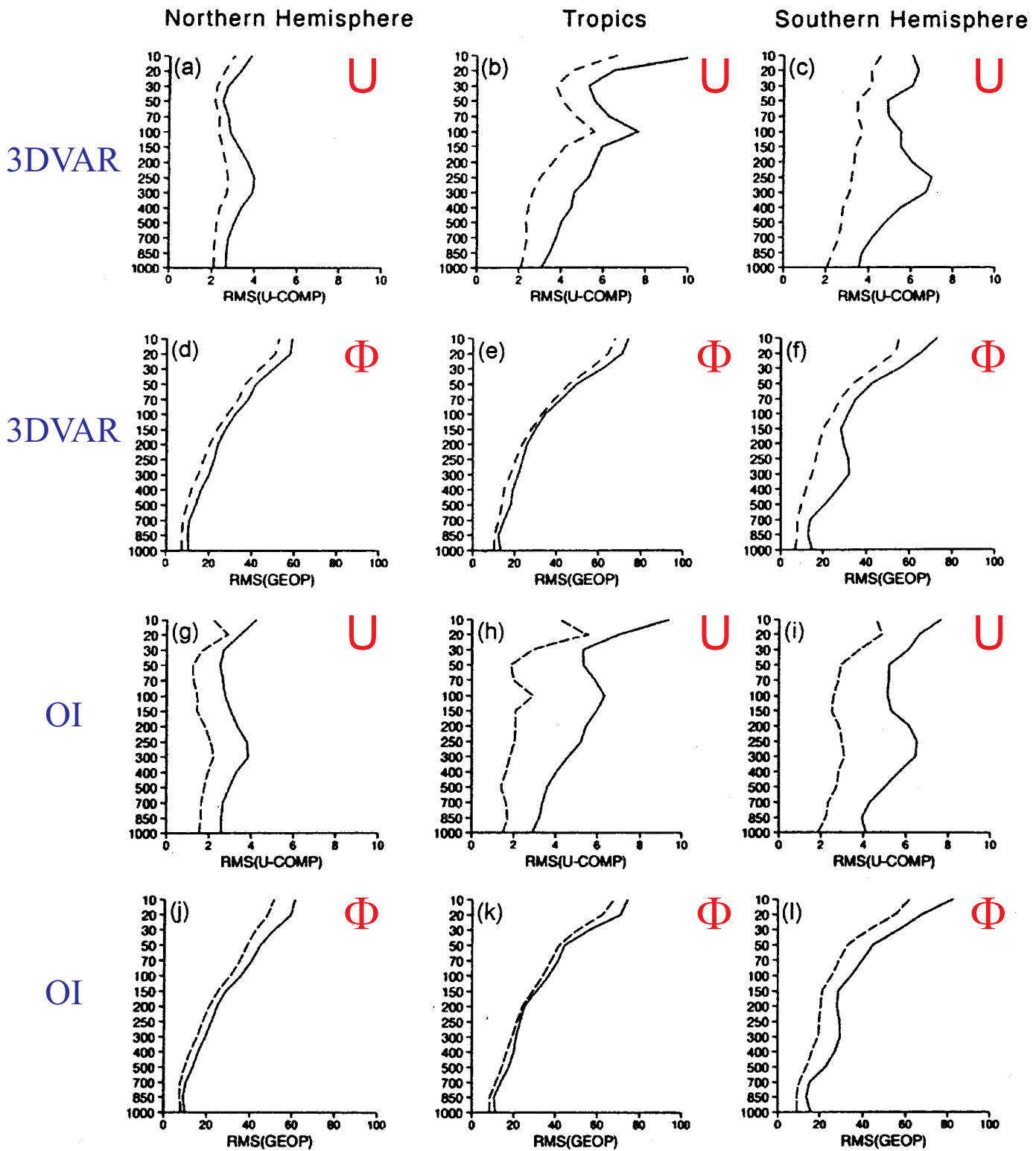**Northern Hemisphere**   **Tropics**   **Southern Hemisphere**

Figure 7. R.m.s. differences at levels from 1000 hPa to 10 hPa for the fourteen-day period 12 UTC 24 August 1995–6 September 1995, between values from all radiosonde data which were used and corresponding values from 3D-Var and OI:

(a) *u* component, 3D-Var, NH; (b) *u* component, 3D-Var, tropics; (c) *u* component, 3D-Var, SH;
(d) geopotential, 3D-Var, NH; (e) geopotential, 3D-Var, tropics; (f) geopotential, 3D-Var, SH;
(g) *u* component, OI, NH; (h) *u* component, OI, tropics; (i) *u* component, OI, SH;
(j) geopotential, OI, NH; (k) geopotential, OI, tropics; (l) geopotential, OI, SH.

NH denotes northern hemisphere north of 20°N, SH denotes southern hemisphere south of 20°S and tropics denotes the region within 20 degrees of the equator. Pecked lines denote observation minus analysis and full lines observation minus background.
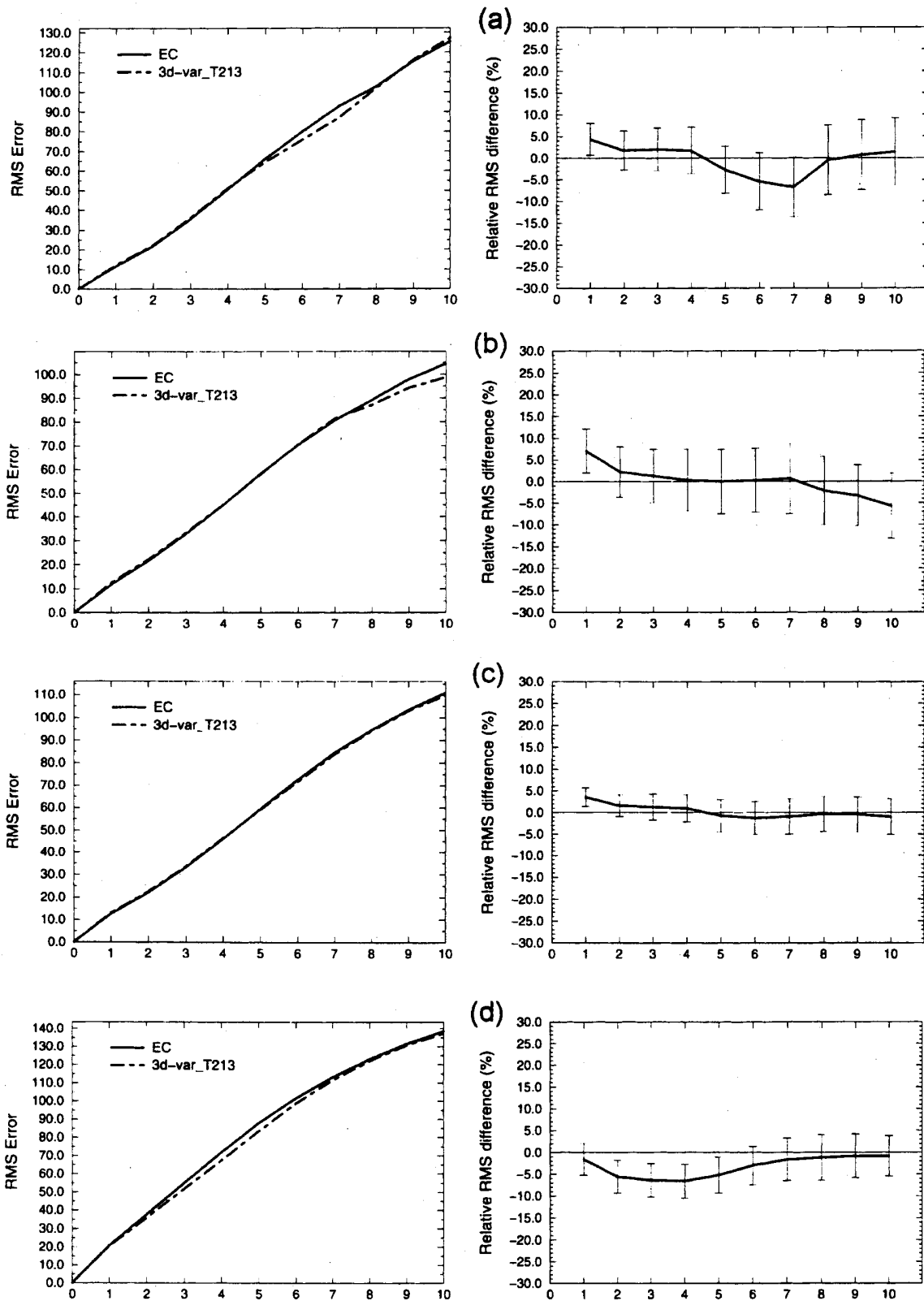
Andersson et al. (1998)

Figure 1.   Average scores for forecasts of geopotential at 500 hPa, from 12 UTC on 120 days in three separate periods (5 April 1995–14 May 1995; 24 August 1995–28 October 1995; 16 January 1996–29 January 1996), verified against their own analyses: (a) Europe; (b) North America; (c) northern hemisphere (north of 20°N); (d) southern hemisphere (south of 20°S). The left-hand plot in each panel shows the r.m.s. error (m), and the right-hand plot the relative r.m.s. difference (per cent). The full line denotes OI and the dashed line 3D-Var.
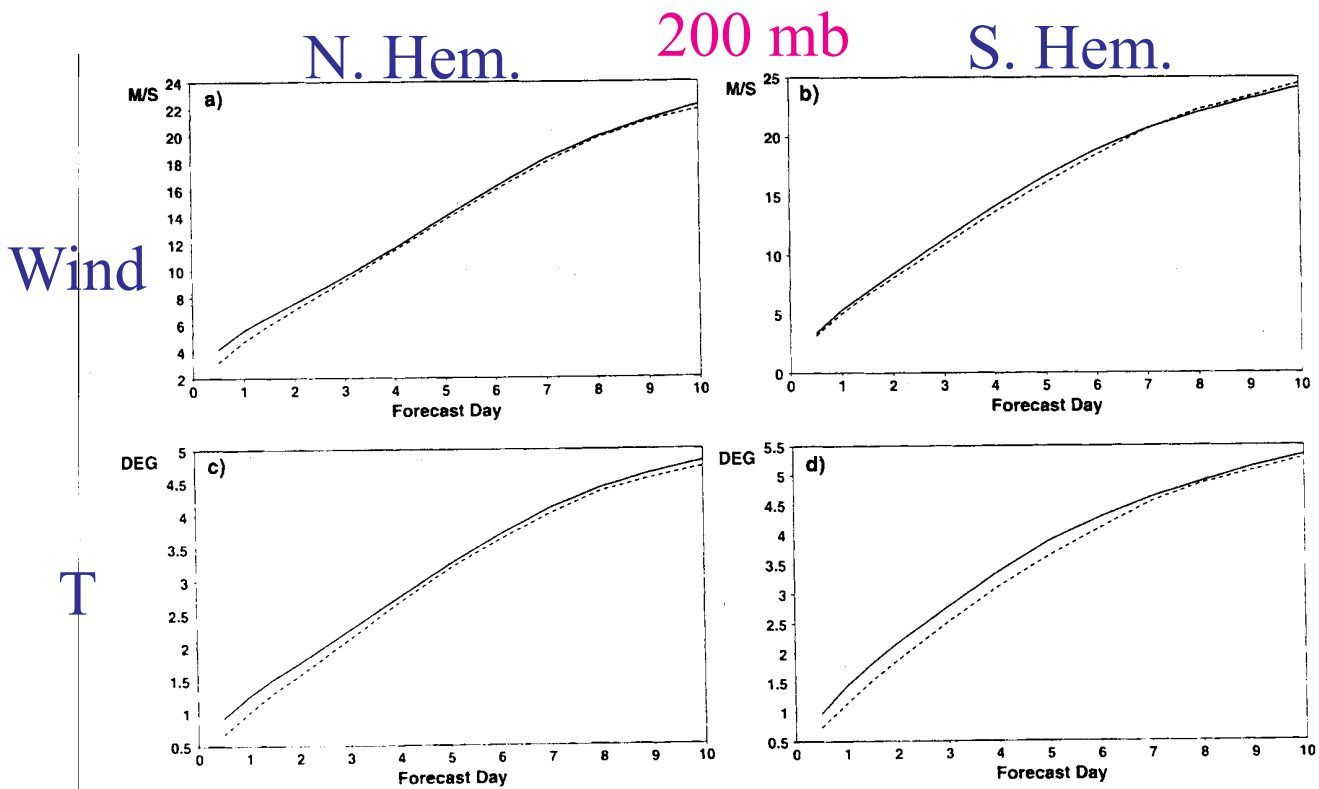
Andersson et al. (1998)

N. Hem. 200 mb S. Hem.

Wind

T

Figure 2.   Average r.m.s. errors of forecasts of wind (m s^{-1}) and temperature (K) at 200 hPa, averaged over 120 days at 12 UTC in three separate periods (5 April 1995–14 May 1995; 24 August 1995–28 October 1995; 16 January 1996–29 January 1996), verified against their own analyses: (a) northern hemisphere wind; (b) southern hemisphere wind; (c) northern hemisphere temperature; (d) southern hemisphere temperature. The full line denotes OI and the dashed line 3D-Var.
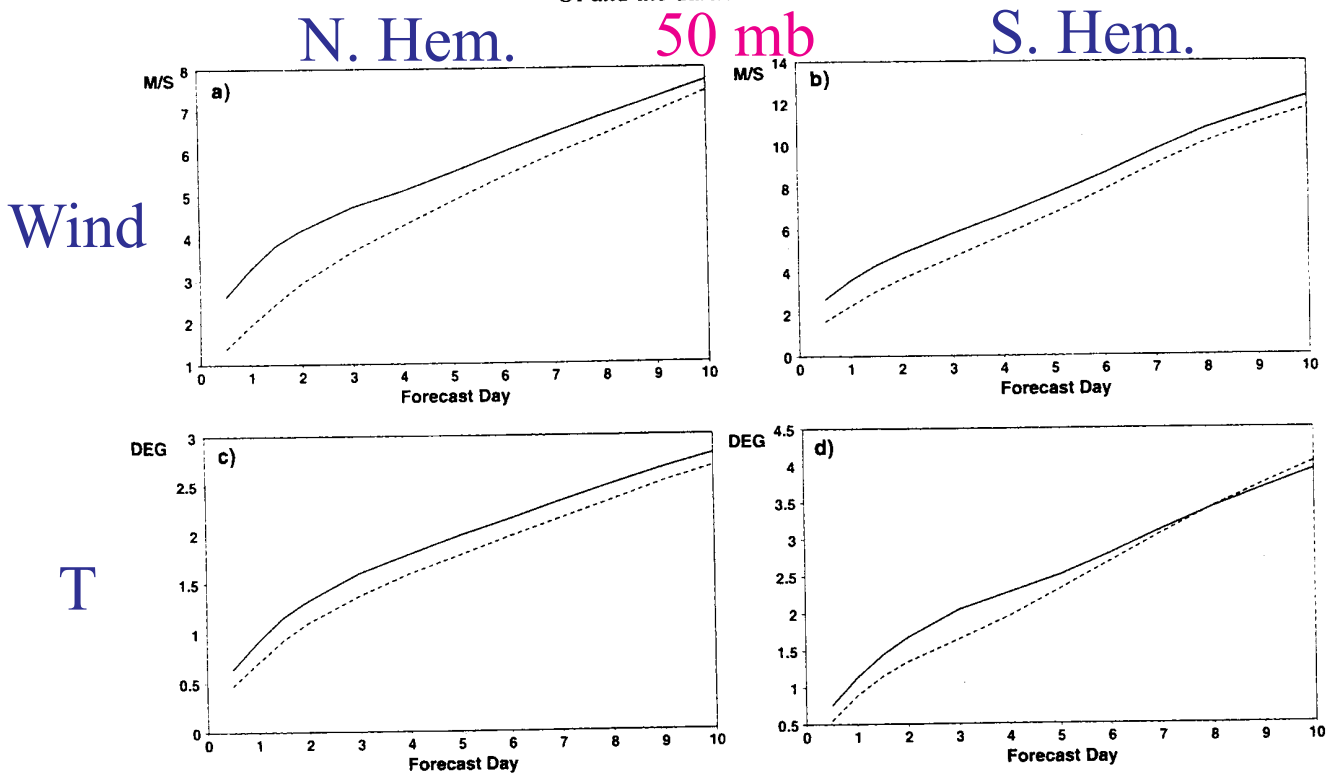
N. Hem. 50 mb S. Hem.

Wind

T

Figure 3.   Average r.m.s. errors of forecasts of wind (m s^{-1}) and temperature (K) at 50 hPa, averaged over 120 days at 12 UTC in three separate periods (5 April 1995–14 May 1995; 24 August 1995–28 October 1995; 16 January 1996–29 January 1996), verified against their own analyses: (a) northern hemisphere wind; (b) southern hemisphere wind; (c) northern hemisphere temperature; (d) southern hemisphere temperature. The full line denotes OI and the dashed line 3D-Var.
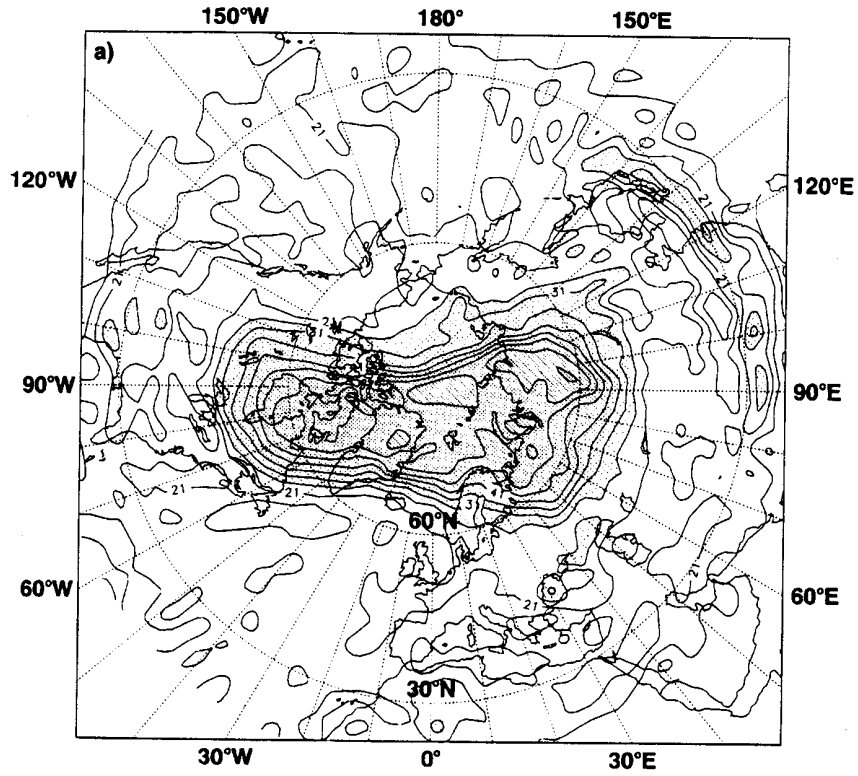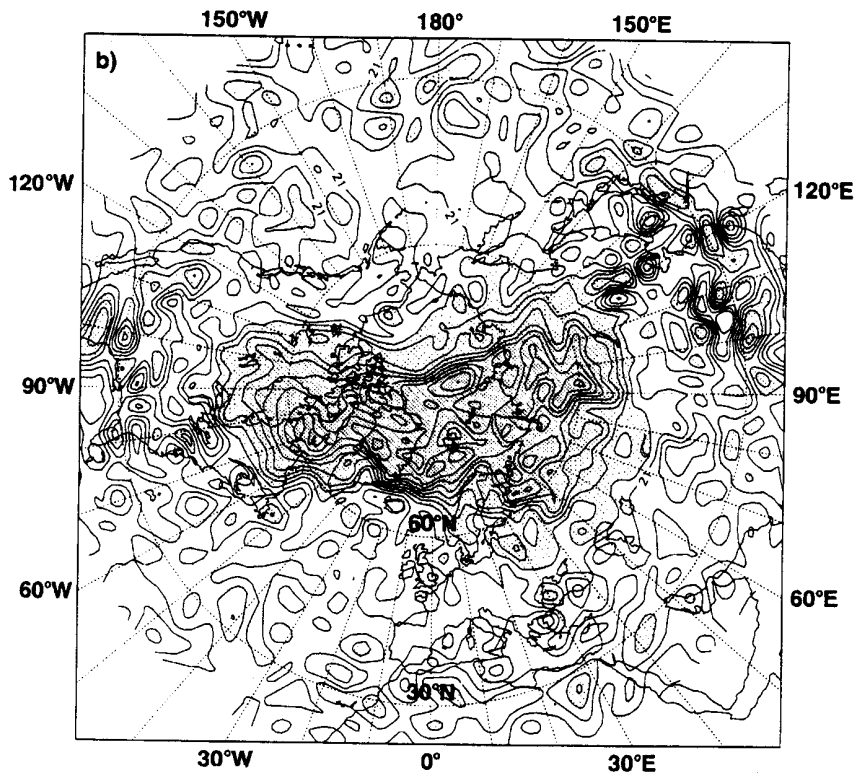
Andersson et al. (1998)

3DVAR

OI

Figure 10. Potential vorticity on the 475 K isentropic surface in northern mid- to high latitudes at 12 UTC 29 January 1996: (a) 3D-Var; (b) OI.
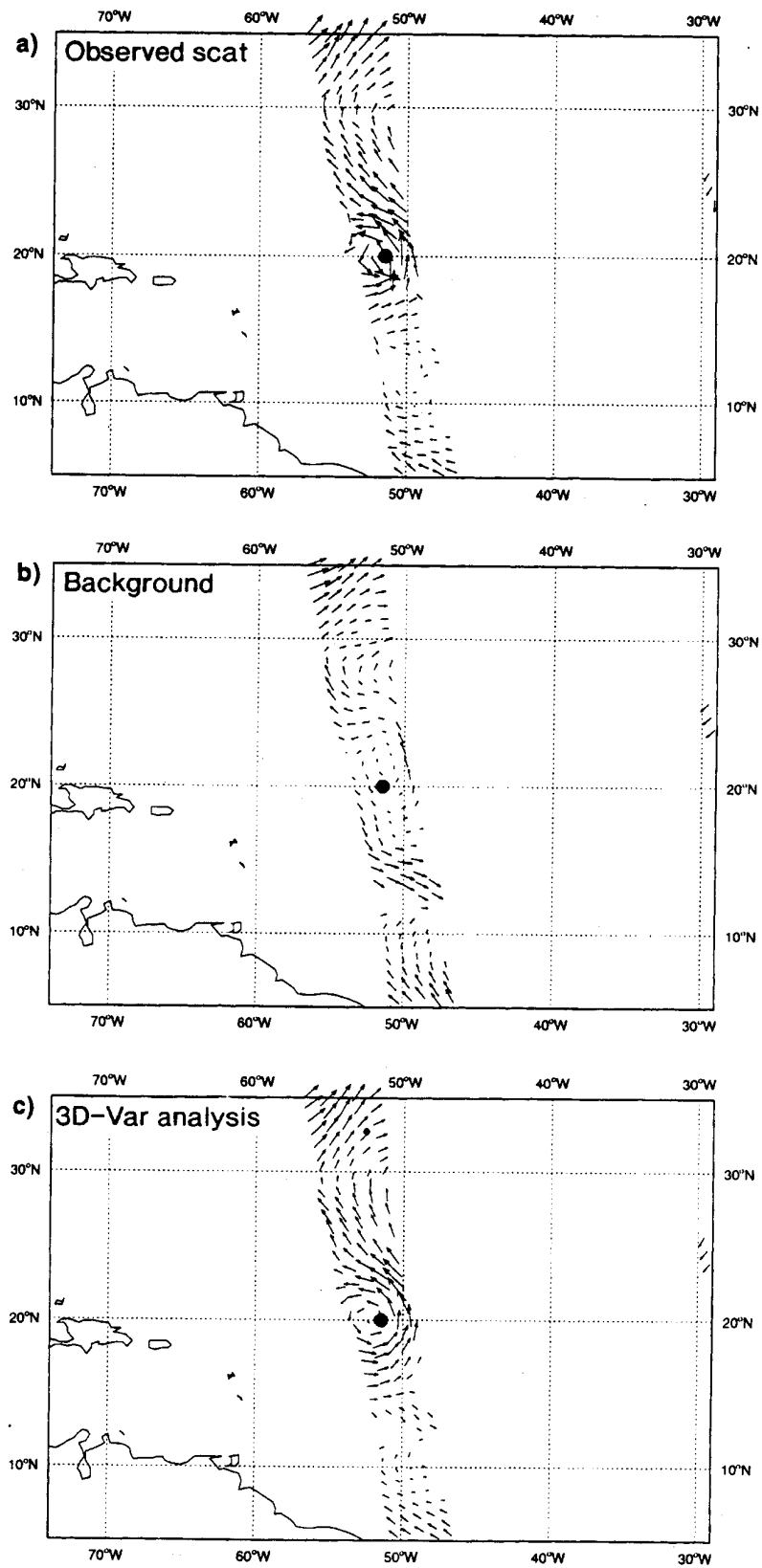
Andersson et al. (1998)

Figure 11. Winds beneath an orbit which passes over tropical cyclone *Karen* located at 20°N, 52°W (large dot) on 31 August 1995: (a) observed by scatterometer; (b) background (six-hour) forecast valid for the same time; (c) 3D-Var analysis. (b) and (c) are interpo;ated to the positions of the scatterometer observations.

Andersson et al. (1998)

NCEP 5-day Forecast Anomaly Correlation (500hPa)
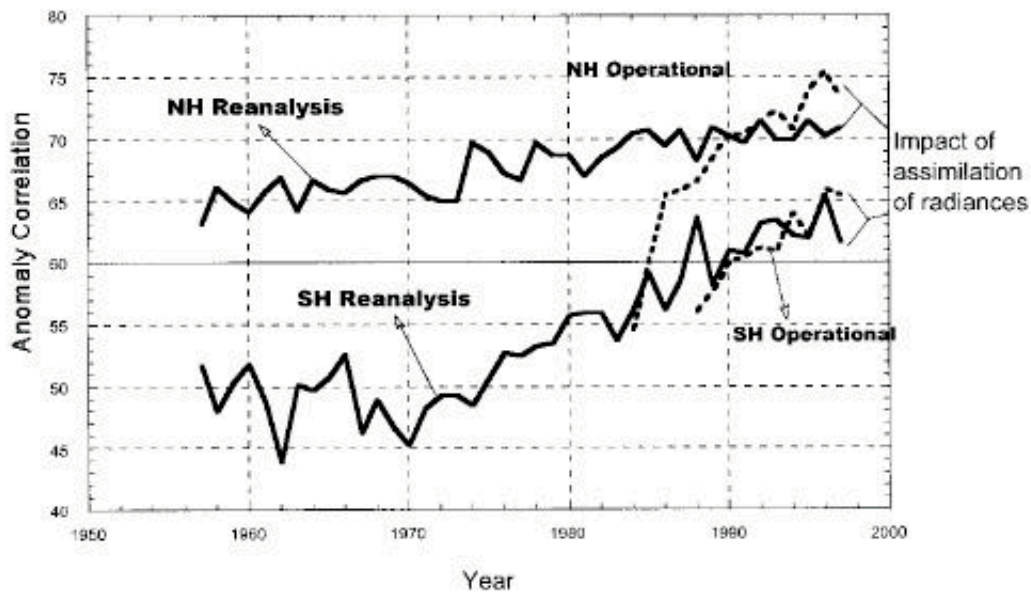Reanalysis and Operational Scores

FIG. 6. Comparison of operational and reanalysis 5-day forecast anomaly correlations for the NH and the SW. The large improvement in operational forecasts observed in 1996–97 is due, to a large extent, to the direct assimilation of TOVS radiances (data courtesy of R. Kistler).

Kalnay et al. (1998)

Anomaly = diff. between a forecast and climatology
Anomaly correlation = pattern correlation between forecast anomalies and verifying analysis anomalies
1974 - improved NESDIS VTPR retrievals
1978 - TOVS retrievals